ELSEVIER

Journal of Structural Geology 29 (2007) 1573–1584

JOURNAL OF STRUCTURAL GEOLOGY

www.elsevier.com/locate/jsg

A mechanical model for complex fault patterns induced by evaporite dehydration and cyclic changes in fluid pressure

Nicola De Paola [a,b,*], Cristiano Collettini [b], Fabio Trippetta [b], Massimiliano R. Barchi [b], Giorgio Minelli [b]

[a] *Reactivation Research Group, Earth Sciences Department, University of Durham, South Road, Durham DH1 3LE, UK*
[b] *Gruppo di Geologia Strutturale e Geofisica, Dipartimento di Scienze della Terra, Università di Perugia, Piazza Università 1, 06100 Perugia, Italy*

Received 5 April 2007; received in revised form 13 July 2007; accepted 27 July 2007
Available online 16 August 2007

Abstract

Complex fault patterns, i.e. faults which exhibit a diverse range of strikes, may develop under conditions where a regional tectonic stress field is weak or absent (e.g. polygonal faults). The present paper considers a complex system of synsedimentary faults in the Umbria-Marche Apennines (Italy), geometrically similar to polygonal fault systems, developed during an early Jurassic extensional episode. This particular fault pattern differs from many extensional fault systems as it lacks structures that are developed with a classical bimodal conjugate ''Andersonian'' geometry. A conceptual and mechanical model is proposed to explain the development and evolution of the complex fault pattern in which it is proposed that faulting is primarily controlled by the development of volumetric instability in Triassic Evaporites due to dehydration processes (anhydritisation) during burial. The lithological architecture of the Triassic Evaporites, comprising interbedded Ca-sulphate layers and dolostones, played a fundamental role in controlling the deformation processes. Cyclic fluid overpressure build-up/release and the coexistence of brittle and brittle-ductile flow processes led to horizontal isotropic and non-plane extensional strain fields within the dehydrating rock mass, which favoured the development of complex deformation patterns. The mechanical model proposed shows that the studied fault pattern developed under a stress field consistent with almost homogeneous stress intensities within the horizontal plane. The data presented show that local strain fields and transient fluid pressure conditions have been dominant over weak regional extensional tectonics. The findings are relevant to many other areas where complex faulting patterns—including polygonal faults—occur in association with evaporite or clay-rich sedimentary sequences.
© 2007 Elsevier Ltd. All rights reserved.

Keywords: Dehydration; Gypsum; Dolomite; Fault reactivation

1. Introduction

Complex fault patterns, i.e. faults which exhibit a diverse range of strikes, differ significantly from simple conjugate Andersonian fault patterns (plane strain), and can develop during a single deformation event in response to: (a) local and/or regional imposed 3-D strain (e.g. the quadrimodal/orthorhombic fault patterns described in Reches, 1978, 1983; Reches and Dieterich, 1983; Krantz, 1988; De Paola et al., 2005a,b,in press; and multiple fault patterns in Nieto-Samaniego and Alaniz-Alvarez, 1997), (b) local stress concentration and reorientation during fracture interaction (e.g. Healy et al., 2006), (c) gravity sliding collapse (Higgs and McClay, 1993; Clausen et al., 1999), (d) density inversion (Henriet et al., 1991; Watterson et al., 2000), (e) syneresis (Cartwright and Dewhurst, 1998; Dewhurst et al., 1999), (f) gravitational loading (Goulty, 2002; Goulty and Swarbrick, 2005), and (g) hydrofracturing and faulting induced by fluid overpressures (Cartwright, 1994). The latter groups of faults (d–g) are commonly referred to as ''polygonal faults'' and they differ from the other groups of complex fault patterns because of their development under

* Corresponding author. Tel.: +44 (0)191 334 2333; fax: +44 (0)191 334 2301.
E-mail address: nicola.de-paola@durham.ac.uk (N.D. Paola).

0191-8141/$ - see front matter © 2007 Elsevier Ltd. All rights reserved.
doi:10.1016/j.jsg.2007.07.015

a weak or absent regional tectonic stress field. Polygonal faults have been observed predominantly in fine-grained sediments (>70% clay content), although the lithologies involved vary from smectite-rich clay to chalk (see a review in Cartwright et al., 2003).

In this paper we investigate whether complex fault patterns, geometrically similar to polygonal fault systems, may develop in response to instability (hydrofracturing and brittle–ductile faulting under high fluid pressure conditions) driven by dehydration reactions of gypsum-bearing rocks during burial. These processes can overwhelm weak regional tectonic strain fields. As an illustrative case study, we describe a complex synsedimentary fault pattern that developed during an early Jurassic extensional episode which is exposed in the Umbria-Marche Apennines of Italy.

2. Geological setting

Three main tectonic phases have affected the Umbria-Marche Apennines since the early Jurassic: (i) Jurassic extension caused the dismembering of the regional carbonate platform (shallow water limestones of the Calcare Massiccio Fm.) and produced the bathymetric differentiation of depositional environments in deep pelagic basins (fault hanging-walls, Fig. 1a,b) and relatively shallow water structural highs (fault foot-walls, Fig. 1a,b); (ii) late Miocene–early Pliocene shortening generated the Umbria-Marche thrust and fold belt (e.g. Barchi et al., 1998a); (iii) late Pliocene–Quaternary extension drove the formation of intramontane continental basins and is responsible for the present-day seismogenic activity in the area (Lavecchia et al., 1994; Barchi et al., 1998b; Decandia et al., 1998).

Seismic reflection profiles crossing the Northern Apennines integrated with borehole data (Barchi et al., 1998b; Collettini and Barchi, 2002; Mirabella et al., 2004) show that the Triassic Evaporite sequences (i.e. Burano Fm., Martinis and Pieri, 1964) are up to 1.5–2 km thick and are interposed between the Permian–Triassic phyllitic basement and the Meso–Cenozoic carbonate multilayer (Barchi et al., 1998b). The mechanical behaviour of the Triassic Evaporites during the Jurassic extension event is still uncertain. In particular, two main roles have been inferred for this unit depending on the particular model proposed to explain the Jurassic fault pattern: (1) a ''passive role'' in which the evaporitic units acted as the detachment horizon for the networks of bimodal and/or quadrimodal (e.g. ''chocolate tablet'' fault patterns of Ramsay and Huber, 1983), high angle listric faults in the carbonate units above (Bally et al., 1986; Alvarez, 1989, 1990); (2) an ''active role'' as diapiric movements and mobilisation by ductile flow of the evaporites triggered faulting and tectonic instability in the carbonate units above (Colacicchi et al., 1970; Santantonio, 1994). Mixed models have been also proposed between these two end-members (e.g. Cooper and Burbi, 1986).

Since the Hettangian/Sinemurian, extensional fault activity dismembered the regional carbonate platform of the Calcare Massiccio formation into several relatively small blocks, with areal extents of only a few km^2, bordered by synsedimentary normal faults (Fig. 1a,b; Colacicchi et al., 1970). The differential tectonic subsidence between fault-bounded pelagic carbonate platforms and basins controlled the deposition of thin (up to few tens of metres) and thick (up to 500–600 m) Hettangian/Sinemurian–Tithonian sedimentary pelagic sequences, respectively (Fig. 1). There is general agreement that the Jurassic extensional event had a peak of activity during the Hettangian/Sinemurian–Pliensbachian and that post-Pliensbachian faulting, during the Jurassic, had only minor effects on the Jurassic synsedimentary fault pattern. This is confirmed by the rapid development of erosional margins as a direct expression of local tectonics during the Hettangian/Sinemurian–Pliensbachian and by the abundant evidence for syn-tectonic activity (i.e. slumps, rock-falls, turbiditic sediments) recorded within the thick sequences of basinal limestones of the Corniola Formation (Hettangian/Sinemurian–Pliensbachian, Fig. 1c) (Passeri, 1971; Bice and Stewart, 1985; Santantonio, 1994; Carminati and Santantonio, 2005). This implies that most of the fault offset (throw) was reached within approximately less than 10 Ma and that it largely determined the submarine relief (Fig. 1b). The exposed normal fault planes underwent strong erosion (paleoescarpments in Santantonio, 1994; Carminati and Santantonio, 2005), which may have caused local disruption and irregular fault geometries (e.g. local spurs and embayment), with only minor changes in fault trend when viewed at a regional scale. The submarine rift topography, mostly produced during the Hettangian/Sinemurian–Pliensbachian, became completely buried in the early Cretaceous, during the deposition of the pelagic limestones of the Maiolica formation (Fig. 1c), when the Jurassic event had already terminated, suggesting underfilling of the hanging-wall pelagic basins (i.e. fault displacement rate > sedimentation rate during the Jurassic event). This allows us to estimate that the decompacted thickness of basinal sections (from the Hettangian/Sinemurian to the early Cretaceous) corresponds approximately to the Jurassic throw which therefore generally did not exceed 500–700 m (Fig. 1b, Santantonio, 1994; Carminati and Santantonio, 2005). Tectonic extension during the early Jurassic has been documented across the entire Italian peninsula, from Southern Alps to Sicily (Ziegler, 1988). However, in the study area, the amount of Jurassic extension (Hettangian/Sinemurian–Pliensbachian) is considered to be relatively minor and is associated with little regional subsidence (Santantonio, 1994).This accords with the limited fault throws and topographic relief in this area compared to other sectors of the Western Thetis paleogeographic domain (see Santantonio et al., 1994 and references therein). In particular, the presence of some regional N–S trending normal fault lineaments (e.g. margin of the Sabina Plateau in figure 1 of Santantonio et al., 1994), suggests that the regional stress field may have been characterised by some E–W weak extension (present day geographic coordinates).

3. The Jurassic fault pattern

The Jurassic fault pattern is exposed in the Umbria-Marche Apennines within the core of regional anticlines, developed during the upper Miocene-lower Pliocene shortening event, where the oldest rocks of the carbonate multilayer crop out

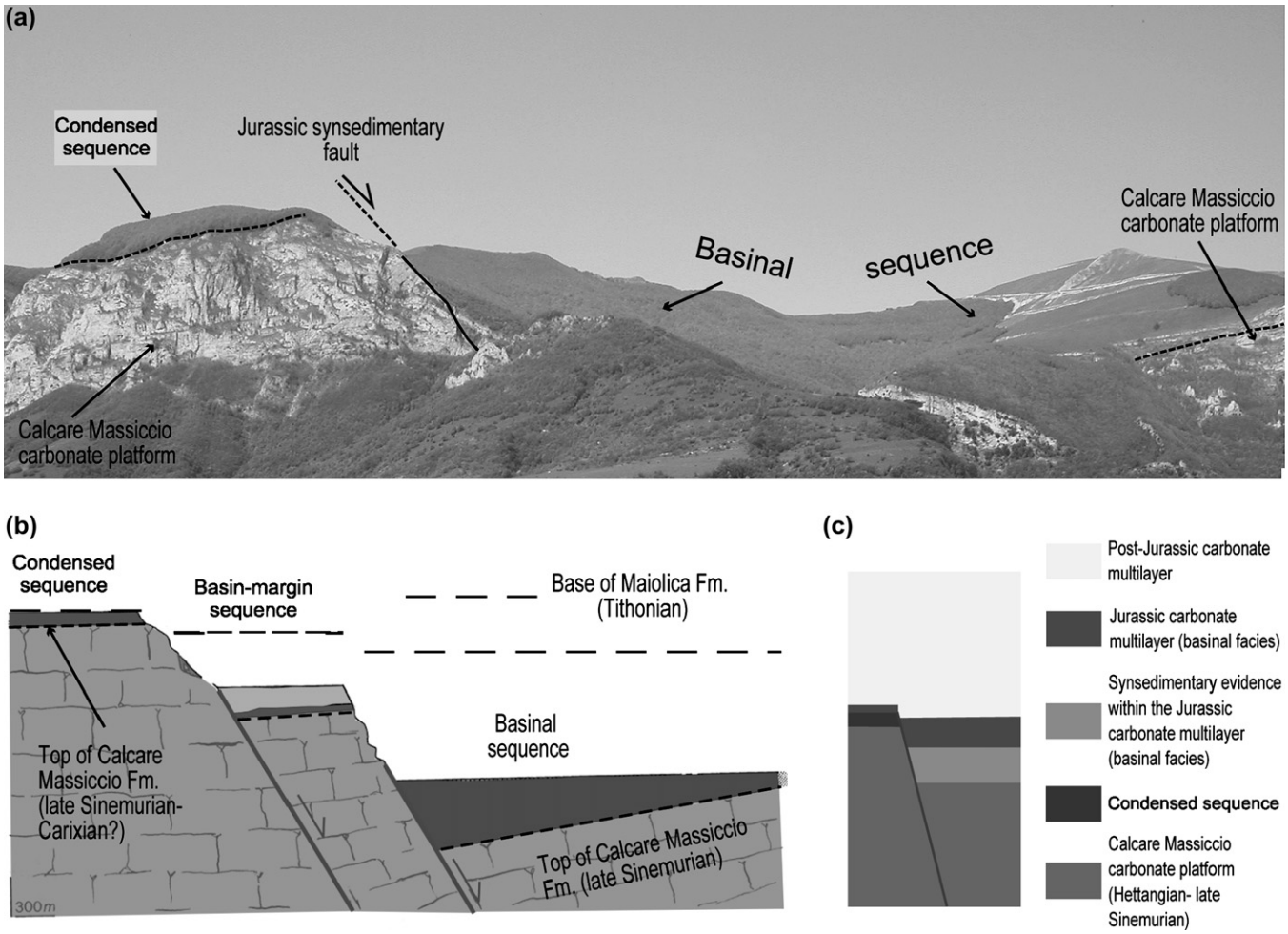

Fig. 1. (a) Field example of a Jurassic synsedimentary fault (location shown in Fig. 2) and associated synsedimentary facies in the hangingwall (basinal sequence) and footwall (condensed sequence), respectively. (b) Schematic representation of the early Jurassic differentiated pelagic environments during the early stages of synsedimentary faulting in the Hettangian/Sinemurian (modified after Santantonio, 1994). (c) Schematic relationship between the earliest syn- (carbonate platform sequence), syn- (condensed and basinal pelagic sequence) and post-Jurassic facies (pelagic sequence).

(Fig. 2a,b). Fault-bounded blocks are in general smaller or have a similar size to the dimensions of the fold cores, allowing for full exposure of most of the mapped fault segments (Fig. 2a,b). There is no exposure at the surface of the Jurassic fault pattern within the regional synclines interposed between the major anticlines, where the youngest, post-Jurassic, deposits of the carbonate multilayer and the syn-orogenic turbiditic sediments of the foreland basins crop out. The curved shape of the Umbria-Marche Apennines is evident from the orientation of the regional anticlines which change from NW-trending in the northern sectors to SW-trending in the southern sectors (Fig. 2a). This affects the orientation of the regional anticline cores and consequently, the exposure of the Jurassic fault patterns (Fig. 2a).

The Jurassic stratigraphic sequences lying between the top of the shallow water limestones of the Calcare Massiccio formation (Hettaangian/Sinemurian) and the bottom of the pelagic limestones of the Maiolica formation (Tithonian), have been digitised at the regional scale using all the available geological maps (Fig. 2). The condensed (top of the ‘‘pelagic carbonate platforms’’), basin margin (slope and backstepping margins) and complete sequences (basinal areas) have been discriminated based on surface exposures (plan view in geological maps) and their thickness has been measured from geological cross sections obtained from the available geological maps. Finally, the exposed Jurassic faults have been digitised (Fig. 2), characterising each fault segment in terms of attitude, length and throw (i.e. vertical displacement), measured on the basis of the thickness change in the Jurassic sedimentary sequence across the faults (‘‘stratigraphic throw’’ of compacted sediments). It should be noted that some of the faults reported in Fig. 2a represent paleoescarpments (e.g. Santantonio, 1994; Carminati and Santantonio, 2005) developed as the result of erosion processes acting on the underlying synsedimentary Jurassic fault. The displacement (stratigraphic throw) of each individual fault typically lies within a constant range of values between about 300 and 500 m, regardless of the fault orientation. This implies that all the structures measured are hierarchically similar.

The analysis of the Jurassic fault pattern shows a prominent scattered orientation (Figs. 2 and 3), which may have been only slightly accentuated, but not controlled by local irregularities in some mapped paleoescarpments of underlying Jurassic

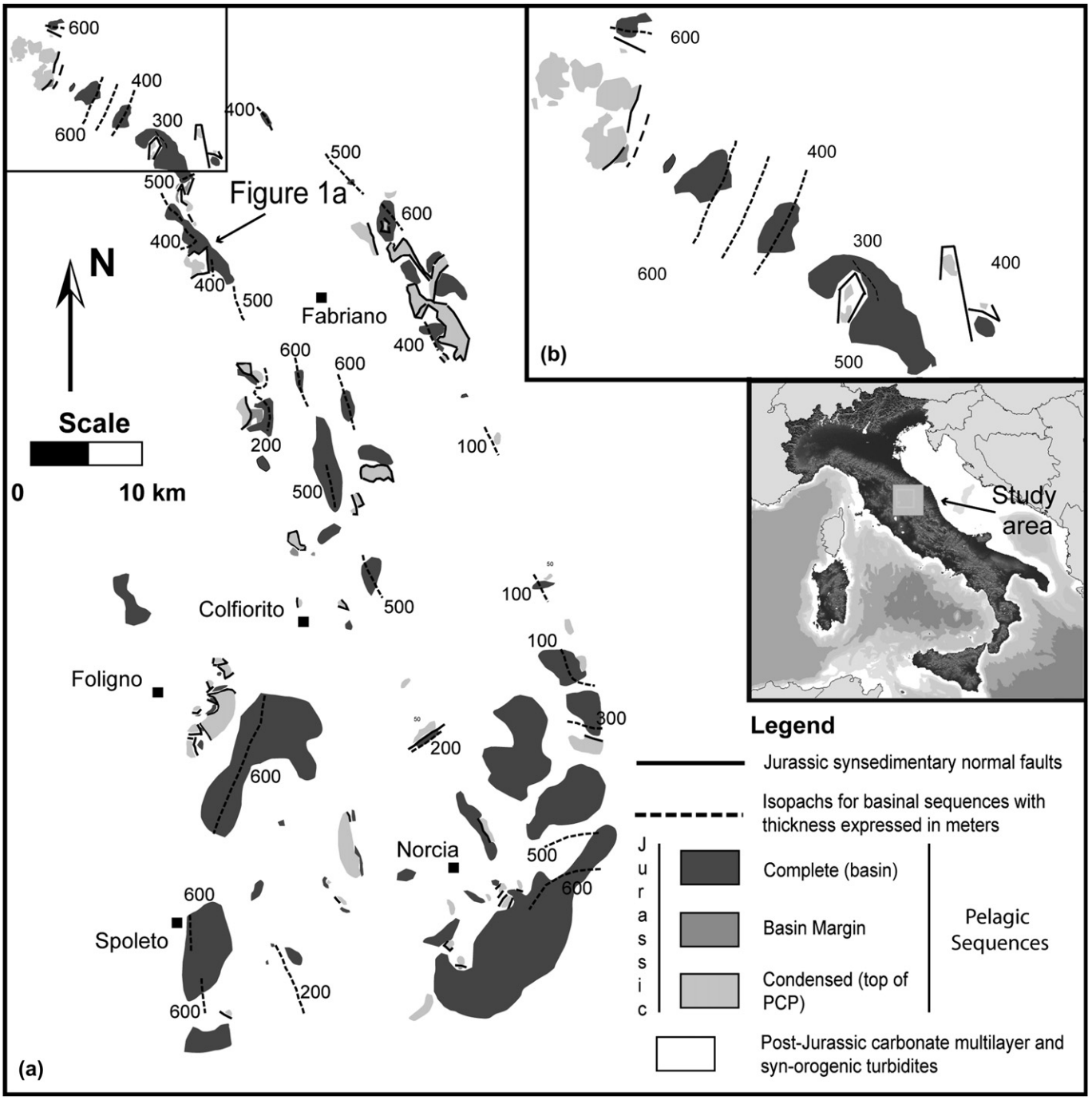

Fig. 2. (a) Structural map of the Umbria-Marche Apennines showing the Jurassic fault pattern (sampled at the cores of the regional anticlines), the thickness and the distribution of the Jurassic basinal facies distinguished in complete, basin margin and condensed. The box (top left) shows the location of b. (b) Enlarged portion of the map showing details about the geometry of the Jurassic fault pattern and associated basinal facies.

normal faults. No ''true'' preferential orientations are observed for the sampled Jurassic faults. The ''apparent'' NW-trending maximum observed on the rose diagram of Fig. 3a, where the fault lengths are plotted, can be explained as being due to the conditions of exposure of the Jurassic fault pattern, which are confined to the cores of the regional anticlines. In fact, most of the Jurassic faults crop out in the northern sectors of the Umbria-Marche Apennines where the major anticlines trend generally NW, generating a bias in the dataset since faults with orientations parallel to the regional folds are exposed with the maximum length. On the other hand, the rose diagram plotted for the number of faults shows no prominent maxima (Fig. 3b) in accord with the observation of a scattered fault pattern. We observe the same scattered orientation for the fault pattern when plotting Jurassic faults within small areas characterised by constant regional fold trend. This evidence shows

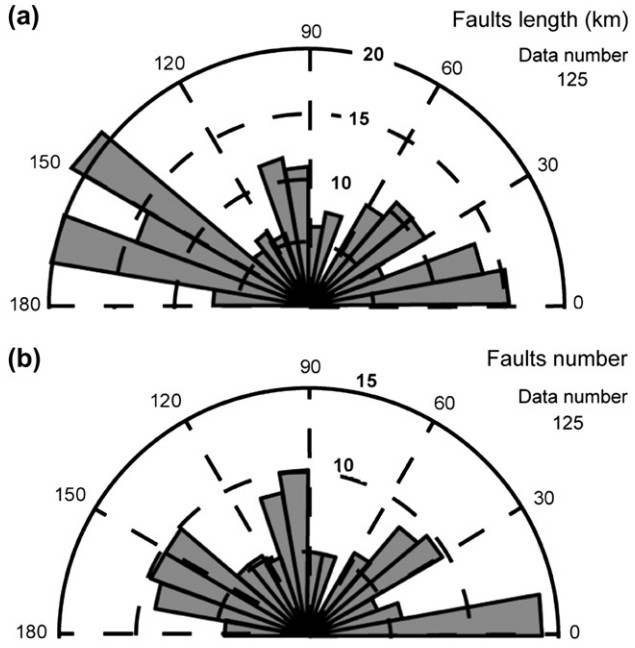

Fig. 3. Rose diagrams of the strike of the Jurassic normal faults mapped in Fig. 2 and plotted as faults length in km (a) and as faults number (b). The dataset shows a largely scattered orientation (see text for details).

that the geometry of the Jurassic fault pattern is unlikely to result from rotations that could have occurred during the late Miocene–early Pliocene evolution of the thrust and fold belt.

The studied fault pattern presents some anomalous aspects compared to classic extensional faults since its development and evolution is significantly different from that expected in a classic bimodal conjugate ''Andersonian'' fault system (plane strain) (Fig. 3). In fact, the direction of maximum extension, orthogonal to the faults, does not cluster with any specific horizontal trend.

4. The geological cycle and history of the Triassic Evaporites dehydration

The Triassic Evaporites formation is a thick sequence, up to 2–2.5 km, composed of decimetric- to decametre scale interbeds of gypsum-anhydrites and dolostones (Fig. 4). Anhydrites were originally deposited as gypsum during the Upper Triassic, in a shallow water environment (Ciarapica and Passeri, 1976; Lugli, 2001). The diagenetic history of the Triassic Evaporites is related to the tectonic conditions during the evolution of the area (Fig. 5). During burial, the gypsum layers become unstable when the increasing pressure and temperature cross the dehydration phase boundary (Fig. 6a), and the gypsum dehydration reaction begins ($CaSO_4 \cdot 2H_2O_{(gypsum)} \rightarrow CaSO_{4(anhydrites)} + 2H_2O$; e.g. Murray, 1964). The gypsum dehydration reaction has a positive Clapeyron slope (Fig. 6a), i.e. the volume of the fluid produced ($\Delta V_{fluid} = +37\%$) is greater than the porosity created by the volume reduction of solids after the dehydration is completed ($\Delta V_{solid} = -30\%$). Jowett et al. (1993) demonstrated that the burial depth of the onset of the gypsum dehydration reaction is controlled by the thermal conductivity of the overlying sediments (lithology) and by the basal heat flow (tectonic environment). The conditions for the beginning of the gypsum dehydration reaction within the Triassic Evaporites should be satisfied at a depth of approximately 700 m (Jowett et al., 1993) if it is assumed that: (a) the mean conductivity of the overlying rocks is 0.0081 cal s^{-1} cm^{-1} K^{-1}, i.e. an average value between gypsum (0.0030 cal s^{-1} cm^{-1} K^{-1}) and dolomite (0.0132 cal s^{-1} cm^{-1} K^{-1}); and (b) the basal heat flow corresponds to

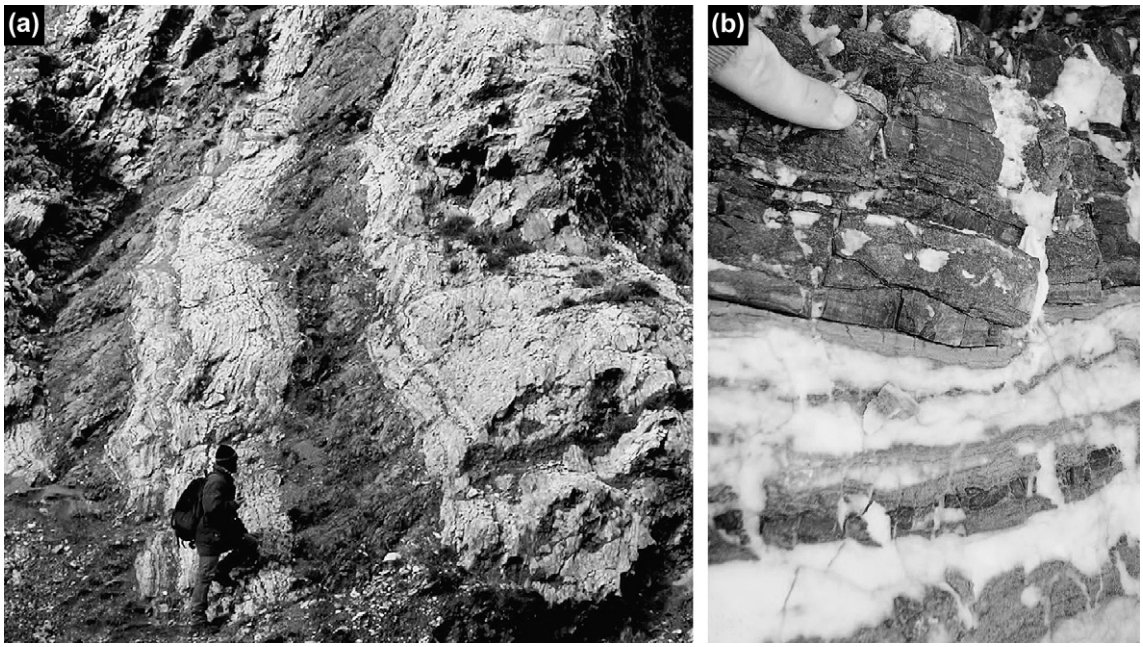

Fig. 4. Triassic Evaporites in the field made of interbedded gypsum and dolostones layers from the metre- (a) to the decimetre-scale (b).

the transition between the rift environment during the Triassic (HFU = 2.0) and the stable passive margin environment during the late Jurassic (HFU = 1.5). Importantly, however, if the dehydration reaction occurs under undrained conditions, i.e. fluids cannot easily escape the system causing a pressure increase, the dehydration process slows down or arrests (Miller et al., 2003). Drained conditions during dehydration, on the other hand, favour the progression of the reaction. At the same time, the kinetics of the gypsum dehydration reaction in a natural system is not well understood. The former unknown factors prevent us from exactly estimating the timing of the onset of the dehydration reaction within the Triassic Evaporites. However, it is reasonable to suggest that when the overlying platform carbonates of the Calcare Massiccio formation reached the critical thickness of about 700 m, during the Hettangian/Sinemurian (Fig. 5), the conditions for the dehydration reaction were satisfied within the entire volume of the Triassic Evaporites. It is interesting to note that the age of the Jurassic extensional event, responsible for the dismembering of the Calcare Massiccio platform during the Hettangian/Sinemurian, coincides with the establishment of such conditions within the entire volume of the Triassic Evaporites (Fig. 5).

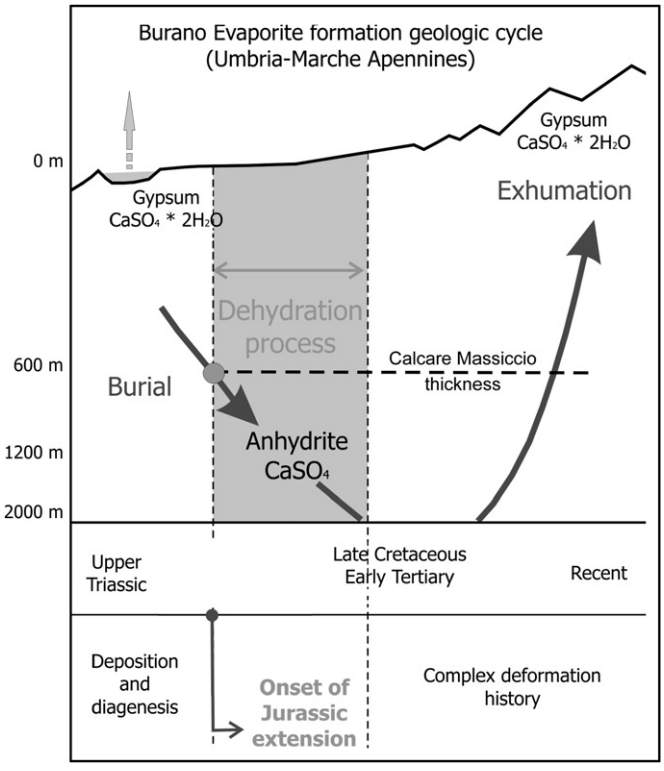

Fig. 5. Geologic cycle of the Triassic Evaporites in the Umbria-Marche Apennines (adapted and modified after Murray, 1964; Lugli, 2001). The Triassic Evaporites have been deposited as alternating gypsum and dolostones in the Upper Triassic within a shallow water environment (Ciarapica and Passeri, 1976). During burial, the dehydration process occurred within the entire volume of the Triassic Evaporites in the Hettangian/Sinemurian, when the Calcare Massiccio reached 600–700 m thickness. This coincides with the onset of the Jurassic extension episode which dismembered the overlying carbonate platform of the Calcare Massiccio. With further burial, the dehydration process must have been completed by the Late Cretaceous–Early Tertiary when more than 2 km of pelagic carbonate rocks were deposited on the top of the evaporites. Gypsum hydration occurs at shallow depths (<1 km), following post-orogenic exhumation and Pliocene–Quaternary extension.

Subsequently, the dehydrated evaporitic rocks have been affected by a complex deformation history since the Early Miocene time when shortening initiated in the westernmost sectors of the Umbria-Marche Apennines (Barchi et al., 1998a). The current diagenetic process affecting this formation is gypsum hydration which is controlled by regional uplift and erosion and exhumation driven by Pliocene–Quaternary extension (Fig. 5). The gypsum hydration occurs at shallow depths (<1 km), as shown by the field observation that most of the Ca-sulphate at the surface is gypsum, and by XRD analyses of cores from boreholes drilled in the Umbria-Marche Apennines which reveal almost pure anhydrite (>95%) below about 1 km depth.

5. Conceptual model

Our conceptual model suggests that Jurassic extension has been strongly influenced by the dehydration of Triassic Evaporites. Laboratory experiments have shown that the expulsion of water during dehydration occurs during three temporally distinct stages (Olgaard et al., 1995; Ko et al., 1997; Miller et al., 2003; Milsch and Scholz, 2005). (1) Fluids initially produced are trapped in isolated, randomly distributed pore networks. This process occurs under undrained conditions within the dehydrating rock mass and results in the development of fluid overpressures ($\Delta V_{\text{fluid}} = +37\%$, $\Delta V_{\text{solid}} = -30\%$). (2) The subsequent development of a connected pore network causes the fluid pressure drop to hydrostatic conditions. During this stage, the maximum water expulsion rate is recorded. (3) Completion of the dehydration reaction results in progressively decreasing water expulsion rates and lower fluid pressures, eventually below hydrostatic levels.

The Triassic Evaporites are affected by different lithologically-controlled deformation processes which are contemporaneous with a weak regional extensional strain field. During burial (increasing pressure and temperature), gypsum dehydration reactivation begins beyond the dehydration phase boundary (Fig. 6a, point B). At this stage, increased pressure (Fig. 6a, point C) can stop the reaction until further thermal energy is input into the system (further burial) or decreased pressure (Fig. 6a, point D) can drive the state of the rock further into the anhydrous phase stable field. In the initial phases of dehydration (Fig. 6a, point B), increasing fluid pressures, especially in areas adjacent to gypsum-dolostones interfaces, causes mechanical weakening (strength reduction and embrittlement) and promotes hydrofracturing and faulting within the dolostone layers (Fig. 6b, stage 1). Brittle deformation within the dolostone rocks causes an increase in crack porosity and permeability, favouring local fluid pressure reductions, thus driving the state of the gypsum-bearing rocks further into the stability field of the anhydrous assemblage (Fig. 6a, point D, e.g. Miller et al., 2003). Fracture opening and slip along faults within the dolostones allow large volumes of fluids to be drained from the dehydrating gypsum layers, through interconnected fracture networks running through pathways of cataclastic fault rocks

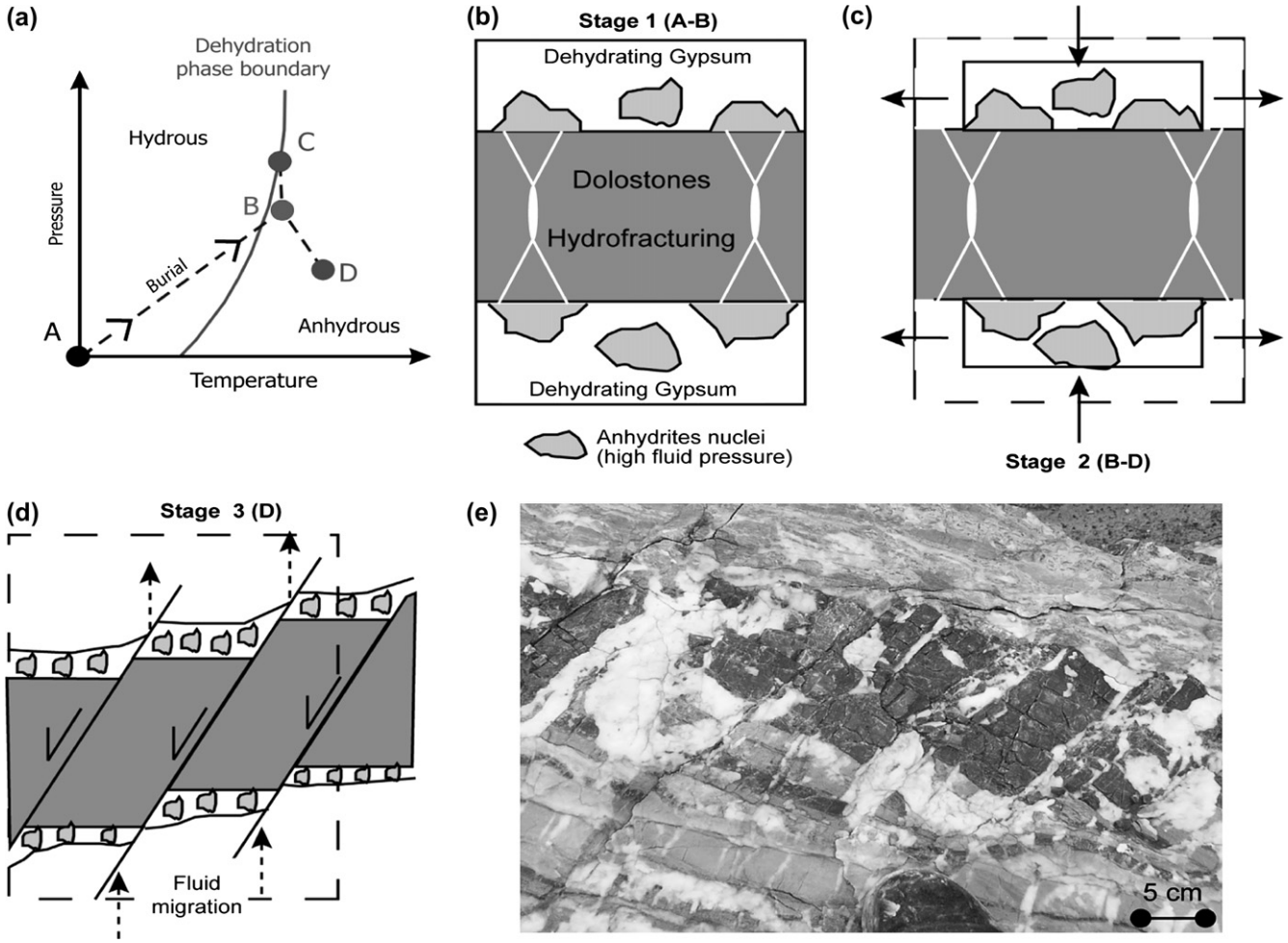

Fig. 6. (a) During burial (increase pressure and temperature), gypsum dehydration reactivation begins beyond the dehydration phase boundary (B). At this stage a pressure increase (C) can stop the reaction until further thermal energy is input into the system (further burial) or a pressure decrease (D) can drive the state of the rock further into the anhydrous phase stable field. (b) The gypsum dehydration reaction increases fluid pressures, trapped at the gypsum–dolostones interface, promoting hydrofracturing and faulting within dolostone rocks. The permeability increases within the dolostone layers and causes fluid discharge. (c) Negative volume change, following fluid expulsion within the dehydrated rocks, causes vertical thinning and isotropic horizontal extension (see text for details). (d) The superposition of brittle (cyclic fracture opening and slip along faults within the dolostones) and ductile (flowage and boudinage within the gypsum–anhydrite rocks) deformation processes favour fault-linkage and upward propagation of the fault system within the Triassic Evaporites. (e) Field example of the interplay between brittle (faulting and fracturing, dark dolostones) and ductile (flowage and boudinage, grey-white gypsum) deformation processes occurring within extending Triassic Evaporites. Note the development of throughgoing normal faults cutting both lithologies.

(Fig. 6b). Fluid drainage results in volume contraction of the dehydrating rocks that is accommodated by vertical thinning and horizontal isotropic extension (Fig. 6c, stage 2). Horizontal isotropic extension, counteracting the horizontal shortening, should prevent the space compatibility problems arising from volume reduction during dehydration (Fig. 6c; e.g. Cartwright, 1994; Cartwright et al., 2003). This state of non-plane strain is accommodated within the composite gypsum–dolostones sequence by mixed deformation processes: flow and boudinage within the ductile gypsum-bearing rocks, and brittle hydrofracturing and faulting within the dolomitic rocks (Fig. 6d,e). Repeated fault reactivation, under transiently increasing fluid pressure conditions, favours fault-linkage and upward propagation of the fault system within the Triassic Evaporites and into the overlying carbonates of the Calcare Massiccio formation (Fig. 6d, stage 3). With further reaction, the increase in porosity and permeability makes drainage more efficient and the pulse of excess pore pressure decreases rapidly (e.g. Olgaard et al., 1995; Ko et al., 1997).

The nature of the described deformation processes predicts the development of a local strain field characterised by isotropic horizontal strain and stress (i.e. $\sigma_2 \approx \sigma_3$).

6. Mechanical model

A 3-D frictional fault reactivation model can be used to infer the state of stress active during the Jurassic time, and the results can then be compared with the orientation of the observed natural fault patterns.

In extending crust the maximum principal effective stress, $\sigma'_1 = (\sigma_1 - P_f)$, is typically vertical and equal to

$$\sigma'_1 = \rho g z - P_f \quad (1)$$

where $\rho = 2750$ kg/m^3 is the average density (Triassic Evaporites plus Calcare Massiccio), g is the acceleration due to gravity, $z = 2000$ m is the crustal depth and P_f is the pore fluid pressure. The crustal depth of 2 km corresponds to the thickness of the Calcare Massicio fm, ~700 m, plus half of the thickness of the Triassic Evaporites, ~1300 m which should be well within the dehydrating volume of rocks during the Jurassic time.

The level of fluid pressure in the crust can be expressed by the pore fluid factor λ that is

$$\lambda = P_f / \rho g z \quad (2)$$

A $\lambda = 0.4$ corresponds to hydrostatic fluid pressure, whilst $0.4 < \lambda < 1.0$ corresponds to supra-hydrostatic fluid pressure and $\lambda = 1.0$ is the lithostatic fluid pressure level.

Once we fix the initial differential stress condition

$$\sigma_3 = 0.7\sigma_1 \quad (3)$$

which is well within the stable field of the evaporitic rocks for pore fluid pressures below the hydrostatic level $\lambda \leq 0.4$ (see Mohr circle in Fig. 7a–c), we can use the stress shape factor $\phi = (\sigma_2 - \sigma_3)/(\sigma_1 - \sigma_3)$ (Angelier, 1984), to relate the horizontal intermediate principal stress σ_2, to the maximum and minimum principal stresses following the equation

$$\sigma_2 = \phi(\sigma_1 - \sigma_3) + \sigma_3 \quad (4)$$

The stress shape factor, φ, is a useful parameter to estimate the ratio of the horizontal stress axes: when $\phi = 0$ then $\sigma_2 = \sigma_3$, implying an isotropic horizontal stress field, whilst when

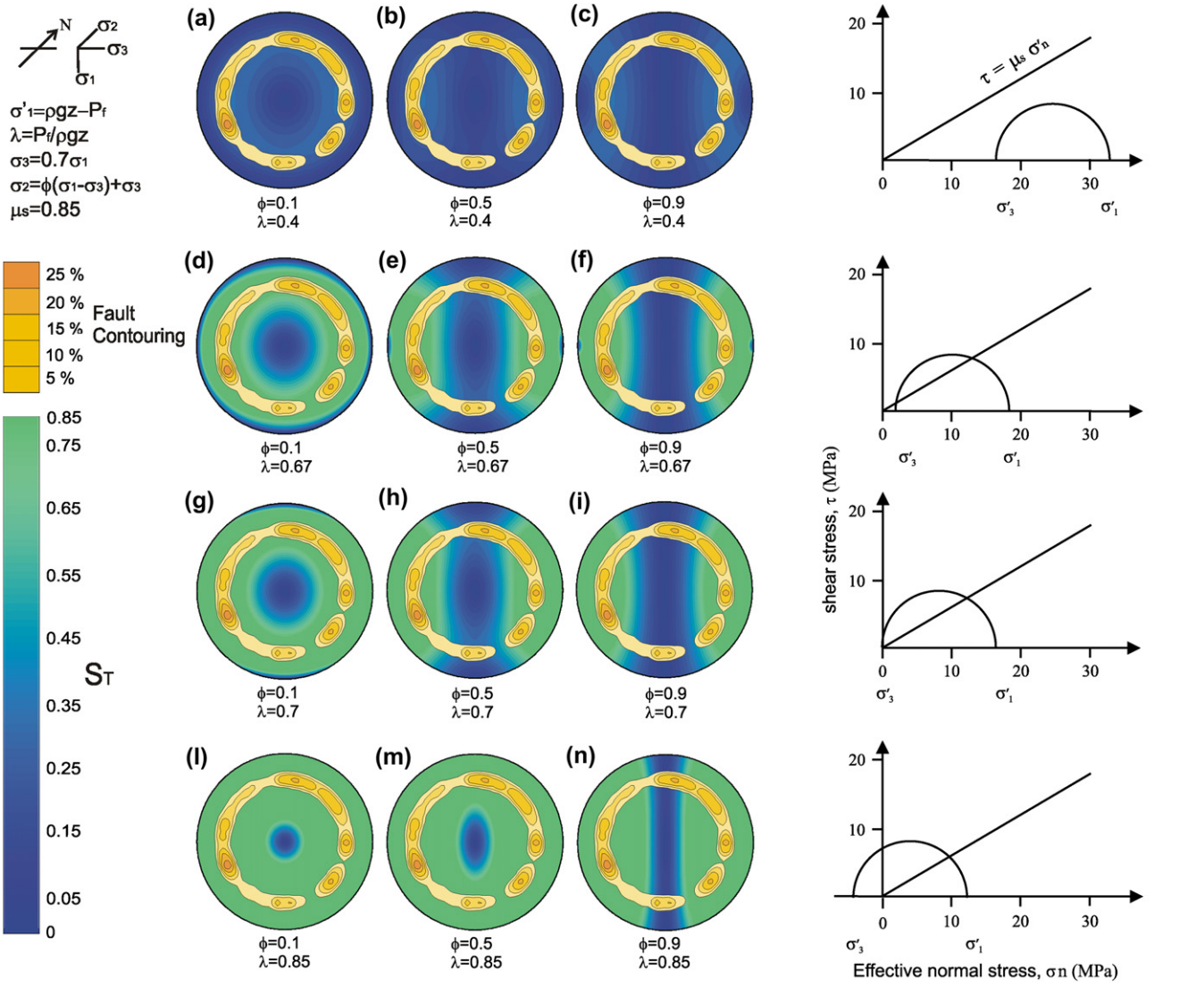

Fig. 7. Slip tendency stereoplot for different values of the pore fluid factor λ and the stress shape factor, φ, plotted against contouring of the Jurassic fault pattern (a–n). Maximum differential stress represented with Mohr circles for fixed λ values (right column). Boundary conditions of the model (top left).

$\phi = 1$, then $\sigma_2 = \sigma_1$, implying that the stress field within the horizontal plane is strongly anisotropic (e.g. Morris et al., 1996; Ramsay and Lisle, 2000 p. 802).

Starting from the stress condition mentioned above, we introduce a 3-D fault reactivation analysis governed by the Amonton's law:

$$\tau = \mu_s \sigma'_n \tag{5}$$

where τ and $\sigma'_n = (\sigma_n - P_f)$ are, respectively, the shear and effective normal stresses acting on the plane of weakness and μ_s is the sliding friction coefficient (Byerlee, 1978). According to this law, frictional stability is determined by the ratio of shear stress to normal stress acting on the plane of weakness. If we define the slip tendency T_s (Morris et al., 1996; Lisle and Srivastava, 2004; Collettini and Trippetta, 2007) as

$$T_s = \tau/\sigma'_n \tag{6}$$

then the following relation

$$T_s \geq \mu_s \tag{7}$$

fixes the condition for frictional instability for each given plane of weakness.

For the given values of the principal stresses σ_1, σ_2, and σ_3, the shear and normal stresses acting on any given plane of the 3-D space depend on the orientation of the planes (Jaeger and Cook, 1979) thus:

$$\sigma'_n = \sigma'_1 n^2 + \sigma'_2 m^2 + \sigma'_3 l^2 \tag{8}$$

$$\tau = \left[\left(\sigma_1^2 n^2 + \sigma_2^2 m^2 + \sigma_3^2 l^2\right) - \sigma'_n 2\right]^{1/2} \tag{9}$$

where n, m and l are the direction cosines of the plane's normal with respect to the principal stress axes σ_1 (vertical in the extending crust) σ_2 and σ_3 respectively.

Slip tendency results can be calculated by solving Eqs. (8) and (9) for the planes in a 3-D space and by substituting the values obtained in Eq. (7) (e.g. Morris et al., 1996; Lisle and Srivastava, 2004; Streit and Hillis, 2004). Contours of T_s can be effectively plotted on equal area stereonets, allowing those fault plane orientations that lie within the frictional instability fields to be visualised directly, i.e. the fault planes for which T_s is higher than the assumed fault friction coefficient μ_s (in Fig. 7 this condition is satisfied for poles to fault planes that plot within the white areas).

For the initial boundary conditions (Eqs. 1–4), the orientation of the planes that satisfy the condition for frictional reactivation is mainly dependent on the orientation of the stress tensor, the friction coefficient μ_s, the fluid pressure P_f and the stress shape ratio $\varphi = (\sigma_2 - \sigma_3)/(\sigma_1 - \sigma_3)$. The orientation of the stress field during the Jurassic time is not known in detail, but on the basis of the previous regional considerations, can be approximately inferred to be characterised by a vertical σ_1, a N–S trending σ_2 and an E–W trending σ_3 (cf. Fig. 7). We adopted a sliding friction coefficient of $\mu_s = 0.85$ (Milsch and Scholz, 2005), which represents a reasonable value for most of the rock types when normal stress $\sigma_n < 200$ MPa (Byerlee, 1978). We assumed for the mapped Jurassic faults a dip range of $60° \pm 10°$ (Fig. 7) which is in accord with field observations (e.g. Santantonio, 1994; Carminati and Santantonio, 2005). It is reasonable to assume that the same dip range applies to the faults within the evaporites since experimental data have shown that faults formed within dolostones and dehydrating gypsum, under low confining pressure, have a dip of about 60° (Olgaard et al., 1995; Austin et al., 2005; Milsch and Scholz, 2005).

Starting from the aforementioned boundary conditions we use slip tendency stereoplots, plotted for different values of fluid pressure (λ) to evaluate the stress shape factor φ that best fits our dataset (Fig. 7). Note that for a fixed σ_1/σ_3 ratio, the crustal depth, z, does not affect the results of our modelling. For all of the values of λ tested, only supra-hydrostatic pore fluid pressures ($\lambda > 0.4$) give a good fit to our dataset (Fig. 7). For $\lambda = 0.4$ (Fig. 7a–c), no values of φ can explain the development of the faults observed in our dataset, whilst for λ values in the range 0.67–0.7 a good fit is obtained for $\phi \leq 1$ and for $\lambda = 0.85$ a good fit is obtained for $\phi \leq 0.5$ (Fig. 8m). However, for $\lambda > 0.7$, fault reactivation can be achieved only under the tensile fluid pressure condition, i.e. $\sigma'_3 < 0$ or $P_f > \sigma_3$ (see Mohr circles in Fig. 7). The tensile fluid pressure condition is difficult to maintain and increases of fluid pressure when $\lambda > 0.7$ would be dissipated by: (i) hydrofracturing when $P_f > \sigma_3 + T$ (Secor, 1965; Sibson, 2000), where T is the rock tensile strength; (ii) high fault zone permeability related to the load-weakening behaviour for normal faulting induced by the decrease of the mean stress (Sibson, 1993) and (iii) the dehydration process generates decreasing values of pore fluid pressure with time (Olgaard et al., 1995; Ko et al., 1997; Miller et al., 2003; Milsch and Scholz, 2005).

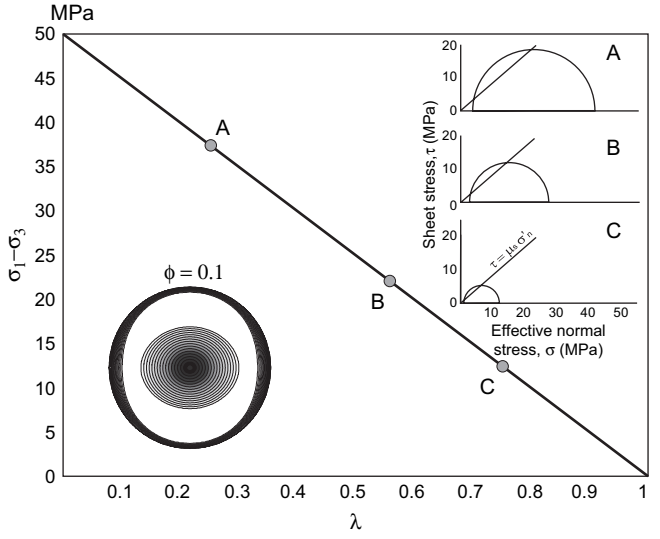

Fig. 8. λ vs. differential stress plot for fixed values of the stress shape factor $\varphi = 0.1$. Each point along the solid line of the graph represents the λ and differential stress values for the slip tendency stereoplot in the bottom left of the diagram. The state of stress is represented by the Mohr circles.

In summary, the mechanical analysis accounts well for the Jurassic faulting pattern under suprahydrostatic fluid pressure and low values of the stress shape factor, a condition that is consistent with the conceptual model predicting an isotropic horizontal state of stress during the Jurassic dehydration episode.

7. Discussion

The mechanical analysis discussed above has been developed for a fixed value of the differential stress, and variable values of pore fluid pressures. This situation applies well to the initial stages of deformation during the Jurassic event, when an increase in pore fluid pressure likely occurs with no changes in the differential stress. However, once faulting continues during the dehydration process, the differential stress tends to increase in response to the reduction of the principal horizontal stress axes (Fig. 6). The solid line on Fig. 8 represents the values of the pore fluid pressure (λ) and the differential stress ($\sigma_1 - \sigma_3$) required to derive the slip tendency stereoplot for $\phi = 0.1$ (Fig. 8). For low values of the differential stress (initial conditions), fault reactivation occurs for high values of λ, suggesting that the triggering faulting mechanism is related to trapped fluid pressures induced by gypsum dehydration. For low values of λ, faulting is induced by increases in differential stress following fluid discharge and the associated vertical thinning and isotropic horizontal extension.

The evolution of the deformation is likely to be complicated and controlled by many local factors and overlapping processes. In particular, factors which may affect and limit locally the increase in pore fluid pressure include the amount of dehydration (Olgaard et al., 1995; Ko et al., 1997), and the fault healing rate and restrengthening (Tenthorey et al., 2003). Other factors may locally affect the decrease in horizontal stresses and change their orientation, such as the amount of fluid discharge and volume change (Cartwright, 1994). Finally the interplay between brittle (faulting and hydrofracturing) and ductile (flowage and boudinage) processes may also influence the structural evolution (Miller et al., 2003). It is evident how, at the local scale, faulting is controlled by the interaction of many parameters which tend to evolve both in space and time during the deformation event. This can result into the development of a fault pattern which tends toward isotropy within the deforming volume of rock, reflecting the influence of local and heterogeneously distributed strain fields over regional, weak strain fields.

Isotropic stress fields within the horizontal plane, similar to the one inferred and discussed in this paper, have been reported from the Danish Central Graben in the North Sea (e.g. Bell, 1996a,b; Ask, 1997). Here wellbore breakout data from the sedimentary cover are extremely scattered and contrast with more uniform stress fields observed further to the north in the Norwegian Sea, where breakouts display a NW–SE orientation, consistent with Atlantic mid-ocean ridge push (Ask, 1997). These data have been interpreted by the aforementioned authors as evidence that the state of stress in the sedimentary cover is influenced by a local stress rather than by platewide stress transmissions. Notably, this area is dominated by diapirism of Zechstein rock salts which may trigger flow-induced ductile deformation processes and pore fluid pressure perturbations (Bell, 1996a,b).

8. Conclusions

We have reconstructed the Jurassic fault pattern of the Umbria-Marche Apennines by discriminating condensed (structural highs) and complete (deeper basins) pelagic sequences. The geometry of the studied Jurassic fault pattern is complex due to the scattered orientation of the faults and the high degree of fragmentation of the fault-bounded blocks. Compared to fault systems active within many other extensional environments, the studied fault pattern does not posses a bimodal conjugate "Andersonian" geometry.

We propose a conceptual and mechanical model for the early Jurassic extensional episode in which deformation is induced by the superposition of a stress field developed due to the dehydration of Triassic Evaporites (anhydritisation) during burial, over a weak regional stress field characterised by minor amounts of E–W extension and little to no regional subsidence. The lithological architecture of the Triassic Evaporites, comprising interbedded layers of gypsum and dolostones, had a fundamental role in controlling the deformation processes and driving the evolution of the fault pattern. In particular, during the initial stage of gypsum dehydration, cyclic fluid overpressure build-up and release triggered hydrofracturing and fluid-assisted faulting within the dolostone layers. Fracturing favoured fluid discharge, leading to drops in pressure and further dehydration reactions. Volume changes induced by dehydration reaction and fluid escape caused a non-plane strain within the evaporites with horizontal isotropic extension and vertical thinning. Coupled brittle and brittle-ductile (ductile flow) deformation processes within the Triassic Evaporites favoured the onset of strain heterogeneities and cyclic fluid overpressures, which were locally driving deformation processes.

Our mechanical model reconstructed the stress field associated with the Jurassic deformation pattern as consistent with an almost isotropic stress distribution within the horizontal plane ($\phi \leq 0.1$) and suprahydrostatic fluid pressures ($\lambda \leq 0.7$). The results of our mechanical modelling explain well the observed fault patterns and can account for the complexity of the deformation processes which overlap both in space and time during the dehydration phase. The data presented show that local and isotropic strain fields, superimposed on a weak regional extension, have strongly controlled the development and evolution of the Jurassic fault pattern.

The model presented here and the case study discussed have significant implications for structural geological studies of faulting in many sedimentary basins around the world from the sub-seismic to regional scales. They are particularly relevant to our understanding of the nature and evolution of fracture interconnectivity and the prediction of fluid flow in hydrocarbon reservoirs in settings where lithologically-controlled brittle faulting and ductile flow occur under transient high fluid pressure conditions, e.g. in basins where there are

significant thicknesses of evaporites and/or argillaceous clasitc sediments. Our findings also suggest that structures geometrically similar to so-called polygonal faults can also develop in evaporites.

Acknowledgements

This study was supported by MIURCofin 2003 Grants, U.R. University of Perugia, Resp. G. Minelli and MIURCofin 2005Grants, U.R. University of Perugia, Resp. C. Collettini. We are grateful to Neil Goulty, Jonathan Imber, Robert Holdsworth, Sergio Llana-Funez and Leonsevero Passeri for comments and improvements of an early version of the manuscript. We have benefited from several useful discussions with Massimo Santantonio, Leonsevero Passeri, Gloria Ciarapica and Simonetta Cirilli. We thank M. Santantonio and D. Dewhurst for their helpful reviews of the paper.

References

Alvarez, W., 1989. Evolution of the Monte Nerone seamount in the Umbria-Marche Apennines: 2. Tectonic control of the seamount-basin transition. Bollettino della Società Geologica Italiana 108, 23–39.

Alvarez, W., 1990. Pattern of extensional faulting in pelagic carbonates of the Umbria-Marche Apennines of central Italy. Geology 18, 407–410.

Angelier, J., 1984. Tectonic analysis of fault slip data sets. Journal of Geophysical Research 89 (B7), 5835–5848.

Ask, M.V.S., 1997. In situ stress from breakouts in the Danish sector of the North Sea. Marine and Petroleum Geology 14 (3), 231–243.

Austin, N.J., Kennedy, L.A., Logan, J.M., Rodway, R., 2005. Textural controls on the brittle deformation of dolomite: the transition from brittle faulting to cataclastic flow. In: Gapais, D., Brun, J.P., Cobbold, P.R. (Eds.), Deformation Mechanisms, Rheology and Tectonics: From Minerals to the Lithosphere. Special Publications 243. Geological Society of London, pp. 51–66.

Bally, A., Burbi, L., Cooper, C., Ghelardoni, R., 1986. Balanced sections and seismic reflection profiles across the Central Apennines. Memorie della Societá Geologica Italiana 35, 257–310.

Barchi, M., DeFeyter, A., Magnani, B., Minelli, G., Pialli, G., Sotera, B., 1998a. The structural style of the Umbria-Marche fold and thrust belt. Memorie della Societá Geologica Italiana 52, 557–578.

Barchi, M., DeFeyter, A., Magnani, M., Minelli, G., Pialli, G., Sotera, B., 1998b. Extensional tectonics in the Northern Apennines (Italy): evidence from the CROP03 deep seismic reflection line. Memorie della Societá Geologica Italiana 52, 528–538.

Bell, J.S., 1996a. Petro Geoscience.1. In situ stresses in sedimentary rocks.1. Measurement techniques. Geoscience Canada 23 (2), 85–100.

Bell, J.S., 1996b. Petro Geoscience 2. In situ stresses in sedimentary rocks.2. Applications of stress measurements. Geoscience Canada 23 (3), 135–153.

Bice, D.M., Stewart, K.J., 1985. Ancient erosional grooves on exhumed bypass margins of carbonate platforms: Examples from the Apennines. Geology 13, 565–568.

Byerlee, J.D., 1978. Friction of rocks. Pure and Applied Geophysics 116, 615–626.

Carminati, E., Santantonio, M., 2005. Control of differential compaction on the geometry of sediments onlapping paleoescarpments: Insights from field geology (Central Apennines, Italy) and numerical modeling. Geology 33, 353–356.

Cartwright, J.A., 1994. Episodic basin-wide fluid expulsion from geopressured shale sequences in the North Sea basin. Geology 22, 447–450.

Cartwright, J.A., Dewhurst, D.N., 1998. Layer-bound compaction faults in fine-grained sediments. Geological Society of America Bulletin 110, 1242–1257.

Cartwright, J., James, D., Bolton, A., 2003. The genesis of polygonal fault systems. In: van Rensbergen, P., Hillis, R., Maltman, A.-J., Morley, C.-K. (Eds.), Subsurface Sediment Mobilization. Special Publications 216. Geological Society of London, pp. 223–243. a review.

Ciarapica, G., Passeri, L., 1976. Deformazione da fluidificazione ed evoluzione diagenetica della formazione evaporitica di Burano. Bollettino della Società Geologica Italiana 95, 1175–1199.

Clausen, J.A., Gabrielsen, R.H., Reksnes, P.A., Nysaether, E., 1999. Development of intraformational (Oligocene-Miocene) faults in the northern North Sea: influence of remote stresses and doming of Fennoscandia. Journal of Structural Geology 21, 1457–1475.

Colacicchi, R., Passeri, L., Pialli, G., 1970. Nuovi dati sul Giurese umbro-marchigiano ed ipotesi per un suo inquadramento regionale. Memorie della Società Geologica Italiana 9, 389–874.

Collettini, C., Barchi, M.R., 2002. A low angle normal fault in the Umbria region (Central Italy): a mechanical model for the related microseismicity. Tectonophysics 359, 97–115.

Collettini, C., Trippetta, F., 2007. A slip tendency analysis to test mechanical and structural control on aftershock rupture planes. Earth and Planetary Science Letters 255, 402–413.

Cooper, M.A., Burbi, L., 1986. The Geology of the Central Sibillini Mountains. Memoriedella Società Geologica Italiana, vol. 35, 323–347.

Decandia, F.A., Lazzarotto, A., Liotta, D., Cernobori, L., Nicolich, R., 1998. The CROP 03 traverse: insights on post-collisional evolution of the Northern Apennines. Memorie della Società Geologica Italiana 52, 413–425.

De Paola, N., Holdsworth, R.E., McCaffrey, K.J.W., Barchi, M.R., 2005a. Partitioned transtension: an alternative to basin inversion models. Journal of Structural Geology 27, 607–625.

De Paola, N., Holdsworth, R.E., McCaffrey, K.J.W., 2005b. The influence of lithology and pre-existing structures on reservoir-scale faulting patterns in transtensional rift zones. Journal of the Geological Society of London 162, 471–480.

De Paola, N., Holdsworth, R.E., Collettini, C., McCaffrey, K.J.W., Barchi, M.R., in press. The structural evolution of dilational step-overs in transtensional zones. Tectonics of Strike-slip Restraining and Realising Bends, Special Volume of the Geological Society of London.

Dewhurst, D.N., Cartwright, J., Lonergan, L., 1999. The development of polygonal fault systems by syneresis of colloidal sediments. Marine Petroleum Geology 16, 793–810.

Goulty, N.R., 2002. Mechanics of layer-bound polygonal faulting in fine-grained sediments. Journal of the Geological Society, London 159, 239–246.

Goulty, N.R., Swarbrick, R.E., 2005. Development of polygonal fault systems: a test of hypotheses. Journal of the Geological Society, London 162, 587–590.

Healy, D., Jones, R.R., Holdsworth, R.E., 2006. Three-dimensional brittle shear fracturing by tensile crack interaction. Nature 439, 64–67.

Henriet, J.P., De Batist, M., Verschuren, M., 1991. Early fracturing of Paleogene clays, southernmost North Sea, relevance to mechanisms of primary hydrocarbon migration. In: Spencer, A.M. (Ed.), Generation, Accumulation and Production of Europe's Hydrocarbons. European Association of Petroleum Geoscientists. Special Publications 1, pp. 217–227.

Higgs, W.G., McClay, K.R., 1993. Analogue sandbox modelling of Miocene extensional faulting in the Outer Moray Firth. In: Williams, G.D., Dobbs, A. (Eds.), Tectonics and Seismic Sequence Stratigraphy. Special Publications 71. Geological Society of London, pp. 141–162.

Jaeger, J.G., Cook, G.W., 1979. Fundamentals of Rock Mechanism, third ed. Chapman and Hall, London, 585 pp.

Jowett, E.C., Cathles, L.M., Davis, B.W., 1993. Predicting depths of gypsum dehydration in evaporitic sedimentary basins. American Association of Petroleum Geologists Bulletin 77, 402–413.

Ko, S., Olgaard, D.L., Wong, T., 1997. Generation and maintenance of pore pressure excess in a dehydrating system. 1. Experimental and microstructural observations. Journal of Geophysical Research 102, 825–839.

Krantz, R.W., 1988. Multiple fault sets and three-dimensional strain: theory and application. Journal of Structural Geology 10, 225–237.

Lavecchia, G., Brozzetti, F., Barchi, M.R., Keller, J.V.A., Menichetti, M., 1994. Seismotectonic zoning in east-central Italy deduced from the

analysis of the Neogene to present deformations and related stress fields. Geological Society of America Bulletin 106, 1107–1120.

Lisle, R.J., Srivastava, D.C., 2004. Test of the frictional reactivation theory for faults and validity of fault-slip analysis. Geology 32, 569–572.

Lugli, S., 2001. Timing of post-depositional events in the Burano Formation of the Secchia Valley (Upper Triassic, Northern Apennines), clues from gypsum-anhydrite transitions and carbonate metasomatism. Sedimentary Geology 140, 107–122.

Martinis, B., Pieri, M., 1964. Alcune notizie sulla formazione evaporitica dell'Italia centrale e meridionale. Memorie della Societá Geologica Italiana 4, 649–678.

Miller, S.A., Van der Zee, W., Olgaard, D.L., Connolly, J.A.D., 2003. A fluid-pressure feedback model of dehydration reactions: experiments, modelling and application to subduction zones. Tectonophysics 370, 241–251.

Milsch, H.H., Scholz, C.H., 2005. Dehydration-induced weakening and fault slip in gypsum: implications for the faulting process at intermediate depth in subduction zones. Journal of Geophysical Research 110, doi:10.1029/2004JB003324. B04202.

Mirabella, F., Ciaccio, M.G., Barchi, M.R., Merlini, S., 2004. The Gubbio normal fault (Central Italy): geometry, displacement distribution and tectonic evolution. Journal of Structural Geology 26, 2233–2249.

Morris, A., Ferrill, D.A., Henderson, D.B., 1996. Slip-tendency analysis and fault reactivation. Geology 24, 275–278.

Murray, R.C., 1964. Origin and diagenesis of gypsum and anhydrite. Journal of Sedimentary Petrology 34, 512–523.

Nieto-Samaniego, A.F., Alaniz-Alvarez, S.A., 1997. Origin and tectonic interpretation of multiple fault patterns. Tectonophysics 270, 197–206.

Olgaard, D.L., Ko, S., Wong, T., 1995. Deformation and pore pressure in dehydrating gypsum under transient drained conditions. Tectonophysics 245, 237–248.

Passeri, L., 1971. Stratigrafia e sedimentologia dei calcari giurassici del M. Cucco (Appennino Umbro). Geologica Romana 10, 93–130.

Ramsay, J.G., Huber, M.I., 1983. Modern Structural Geology. In: Strain Analysis, Vol. I. Academic Press, London. 0–308.

Ramsay, J.G., Lisle, R.J., 2000. Applications of Continuum Mechanics in Structural Geology. In: The Techniques of Modern Structural Geology, Vol. 3. Academic Press. 701–1061.

Reches, Z., 1978. Analysis of faulting in three-dimensional strain field. Tectonophysics 47, 109–129.

Reches, Z., 1983. Faulting of rocks in three-dimensional strain field II. Theoretical analysis. Tectonophysics 95, 33–156.

Reches, Z., Dieterich, J., 1983. Faulting of rocks in three-dimensional strain field I. Failure of rocks in polyaxial, servo-control experiments. Tectonophysics 95, 111–132.

Santantonio, M., 1994. Pelagic carbonate platforms in the geologic record: their classification, and sedimentary, and paleotectonic evolution. American Association of Petroleum Geologists Bulletin 78, 122–141.

Secor, D.T., 1965. Role of fluid pressure in jointing. American Journal of Science 263, 633–646.

Sibson, R.H., 1993. Load-strengthening versus load-weakening faulting. Journal of Structural Geology 15, 123–128.

Sibson, R.H., 2000. Fluid involvement in normal faulting. Journal of Geodynamics 29, 469–499.

Streit, J.E., Hillis, R.R., 2004. Estimating fault stability and sustainable fluid pressures for underground storage of CO_2 in porous rock. Energy 29, 1445–1456.

Tenthorey, E., Cox, S.F., Todd, H.F., 2003. Evolution of strength recovery and permeability during fluid-rock reaction in experimental fault zones. Earth and Planetary Science Letters 206 (1-2), 161–172.

Watterson, J., Walsh, J., Nicol, A., Nell, P.A.R., Bretan, P.G., 2000. Geometry and origin of a polygonal fault system. Journal of the Geological Society of London 157, 151–162.

Ziegler, P.A., 1988. Evolution of the Arctic-North Atlantic and the Western Tethys. American Association of Petroleum Geology Memoirs 43, 198 P. and 30 plates.